



A 2D coupled hydro-thermal model for the combined finite-discrete element method

Chengzeng Yan¹ · Yu-Yong Jiao¹ · Shengqi Yang²

Received: 9 December 2017 / Accepted: 28 March 2018 / Published online: 13 April 2018
© Springer-Verlag GmbH Germany, part of Springer Nature 2018

Abstract

Based on the combined finite-discrete element method (FDEM), a two-dimensional coupled hydro-thermal model is proposed. This model can simulate fluid flow and heat transfer in rock masses with arbitrary complex fracture networks. The model consists of three parts: a heat conduction model of the rock matrix, a heat-transfer model of the fluid in the fracture (including the heat conduction and convection of fluid), and a heat exchange model between the fluid and rock at the fracture surface. Three examples with analytical solutions are given to verify the correctness of the coupled model. Finally, the coupled model is applied to hydro-thermal coupling simulations of a rock mass with a fracture network. The temperature field evolution, the effect of thermal conductivity of the rock matrix thermal conductivity and the fracture aperture on the outlet temperature are studied. The coupled model presented in this paper will enable the application of FDEM to study rock rupture driven by the effect of hydro-thermo-mechanical coupling in geomaterials such as in geothermal systems, petroleum engineering, environmental engineering and nuclear waste geological storage.

Keywords Finite-discrete element method (FDEM) · Fracture flow · Heat conduction and convection · Hydro-thermal coupling · Numerical simulation

List of symbols

q_i	Heat flow rate in the i direction
k_{ij}	Thermal conductivity tensor of rock matrix
T	Temperature
M	Mass
Q_{net}	Net heat flowing into mass M per unit time
t	Time
C_s	Specific heat of rock matrix
A	Area of a triangular element
n	Outer normal vector

\bar{T}^m	Average temperature of edge m
Δx_j^m	Difference between the coordinate components of the two vertices at edge m
\in_{ij}	Two-dimensional permutation tensor
q_x	Heat flow rate along the x direction
q_y	Heat flow rate along the y direction
$n_i^{(n)}$	Outer normal unit vector of the edge opposite to node n
$L^{(n)}$	Length of the edge opposite to node n
$Q_{\Delta 123}$	Heat flow flowing into node 1 from triangular element $\Delta 123$
Q_s	Total heat flow into node 1 per unit time
T_t^s	Nodal temperature at t
$T_{t+\Delta t}^s$	Nodal temperature at $t + \Delta t$ and t
ρ_s	Mass density of rock matrix
V_s	Rock matrix volume of node 1
Δx	Size of the smallest element
h	Convective heat-transfer coefficient
κ	Thermal diffusion coefficient ($k/\rho C_p$ when $k_x = k_y$)
ΔT	Temperature difference between node 1 and node 2
T_1	Temperature at node 1
T_2	Temperature at node 2

✉ Yu-Yong Jiao
yyjiao@cug.edu.cn

Chengzeng Yan
yancz@cug.edu.cn; yanchengzheng86@gmail.com

¹ Faculty of Engineering, China University of Geosciences, Wuhan 430074, China

² State Key Laboratory for Geomechanics and Deep Underground Engineering, China University of Mining and Technology, Xuzhou 21116, China

k_f	Thermal conductivity of fluid
Q_{f1}	Total heat flow rate due to heat conduction
q_f	Fluid flow rate between node 1 and node 2
p_1	Pressure at node 1
p_2	Pressure at node 2
Δp	Pressure difference between node 1 and node 2
μ	Dynamic viscosity of fluid
a	Aperture of fractures
Q_{f2}	Total heat flow rate of node 1 due to heat convection
T_t^f	Temperature of node 1 at t
$T_{t+\Delta t}^f$	Temperature of node 1 at $t + \Delta t$
C_f	Specific heat of fluid
ρ_f	Mass density of fluid
Q_f	Total heat flow rate of node 1
Δt	Time step
V	Half of the volume of all the broken joint elements that connect to node 1
T_s^+, T_s^-	Temperature of rock matrix at both sides of a fracture
T_f	Temperature of fluid in a fracture
L	Fracture length
Q_e	Heat exchange between fluid and rock matrix per unit time
T_L	Temperature of the left boundary
T_R	Temperature of the right boundary
\hat{T}	$(T - T_L)/T_L$
P_e	Peclet number
v_f	Flow velocity of fluid
k_s	Thermal conductivity of rock matrix
T_{s0}	Initial temperature of rock matrix
T_{f0}	Fluid temperature at the left boundary
$erfc$	Complementary error function
μ	Dynamic viscosity of fluid

1 Introduction

The hydro-thermal coupling process in fractured rock mass is a frequently encountered problem in petroleum and geothermal development, disposal of nuclear waste, geological storage of carbon dioxide (CO₂), the prevention and control of high-temperature thermal damage in deep mining, the stability analysis of soft rock tunnel in cold regions. Since the problem has significant theoretical value as well as broad prospects for engineering applications, many researchers have studied the hydro-thermal coupling problem of fractured rock masses in the past 30 years. For example, Barton et al. [2] conducted a preliminary study on

the coupling effect between seepage field, stress field, and temperature field of rock mass. Rutqvist [34] linked the tough family multiphase fluid and heat transport codes with the commercial FLAC3D geomechanical simulator for modeling coupled multiphase flow, heat transport, and geomechanics. Sun et al. [38] presented a mathematical model incorporating the thermal–hydraulic–mechanical (THM) coupling effect to simulate a fractured enhanced geothermal systems (EGS) reservoir in which the geothermal reservoir is regarded as fractured porous media consisting of rock matrix and discrete fractures. Moreover, an international co-operative research project has been established under the name DECOVALEX for theoretical and experimental studies of coupled thermal, hydrological, and mechanical processes in hard rocks [7, 13, 40]. However, the study of coupling between the seepage field and temperature field (i.e., hydro-thermal coupling) of fractured rock mass is relatively few.

In the experimental research of hydro-thermal coupling, Zhao [48] studied the convective heat transfer and water flow in rough granite fractures through experimental investigation. Xu et al. [41] developed a large-scale hydraulic fracturing simulation system for hot dry rock under high-temperature and high-stress conditions. This system can perform experiments of fluid flow in fractures and heat transfer between the fluid and rock under different temperature conditions.

In the numerical study of hydro-thermal coupling, Pruess [32] studied the heat and mass transfer problems between bedrock and fracture, and the effect of bedrock permeability and fracture aperture on heat transfer by numerical simulation. Abdallah et al. [1] proposed a thermal convection model into the universal distinct element code (UDEC) [10] to study the heat transfer caused by fluid circulation through the fractures in rock masses. Tomac, Gutierrez [39] presented the formulation, and implementation of a novel convective heat convection model in the particle flow code (PFC) [8]. Shaik et al. [36] developed a numerical procedure coupling fluid flow with heat transfer and investigated the effect of heat transfer between rock matrix and circulating fluid on economic hot water production from fractured geothermal systems. Jiang et al. [12] presented a three-dimensional transient model for the study of subsurface thermo-hydraulic processes during EGS heat extraction, in which the local thermal non-equilibrium between rock matrix and the fluid flowing in the porous heat reservoir is considered. Xu et al. [42] proposed a simplified approach to simulate the coupled hydro-thermal system based on an equivalent pipe network model. Cui et al. [5] presented the coupled thermo-hydraulic governing formulation as well as the coupled

thermo-hydraulic boundary condition for studying convection-dominated heat transfer in ground source energy systems, such as open-loop systems.

The above hydro-thermal coupling models are either based on continuum or discontinuum. The coupled hydro-thermal model based on continuum is difficult to characterize the special conductivity effect of fractures. Although the discontinuous-based hydro-thermal coupling model can consider a large number of fractures in rock mass, it is difficult to consider crack initiation and propagation when extended to THM couplings.

Therefore, based on the study of Tomac [39] and Shaik [36], this paper presents a coupled hydro-thermal model for the combined finite-discrete element method (FDEM)—an excellent continuous–discontinuous method for simulating rock rupture [26, 28]. This novel coupled hydro-thermal model not only can explicitly consider the fluid flow and heat transport in fractured rock mass, but also can easily extend to the cases of coupled THM (including rock rupture). This paper focuses on the formulation and implementation of the coupled hydro-thermal model in FDEM. The use of the model in coupling THM FDEM modeling will be described in another publication.

FDEM combines the advantages of the finite element method in simulating deformation of solid and the discrete element method in handling contact interaction between blocks. Moreover, the method can simulate crack initiation and propagation by breaking joint elements. In recent years, FDEM and the FDEM code Y [26, 27] have been widely used in the field of rock mechanics, especially in studies of rock rupture [14, 16, 18, 21, 23, 25, 29, 33, 35, 44]. For example, Lei, Rougier and Knight have conducted a lot of interesting research in this area [15, 19, 20]. However, this method can be used for only pure mechanical calculations and cannot be used to address hydro-mechanical coupling problems and hydro-thermal coupling problems. Therefore, some researchers combine FDEM with other software or directly construct the coupled hydro-mechanical model or coupled thermo-mechanical model in FDEM [17, 22, 24, 43–47]. However, FDEM still cannot deal with the coupled hydro-thermal problems. Therefore, a 2D coupled hydro-thermal model (FDEM-TH) based on FDEM is proposed in this paper for simulating heat transfer between fluid and rock. Combining the advantage of FDEM in simulating the deformation and rupture of rock, this coupled hydro-thermal model can be easily extended to the case of coupling THM (including rock rupture).

This paper is organized as follows: First, the heat conduction model of rock matrix is introduced. Secondly, the heat conduction and convection model of fluid in fracture are presented. Then, the heat exchange model between fluid and rock matrix at fracture is presented. Combining

the above three parts, a coupled hydro-thermal model is constructed directly in FDEM. Finally, three examples with analytic solution are given to verify the correctness of the coupled hydro-thermal model. Moreover, an example of hydro-thermal coupling in fractured rock mass is given. The temperature distribution in the rock mass and the effect of rock thermal conductivity and fracture aperture on the outlet fluid temperature are investigated.

2 Heat-transfer model

2.1 Heat conduction model of rock matrix

According to Fourier's law of heat transfer, the heat flow rate in the i direction per unit area can be expressed as:

$$q_i = -k_{ij} \frac{\partial T}{\partial x_j} \quad (1)$$

where q_i is the heat flow rate along i direction, k_{ij} is the tensor of the thermal conductivity of the rock matrix, and T is the temperature.

For any given mass M , the temperature change can be written as [11]

$$\frac{\partial T}{\partial t} = \frac{Q_{\text{net}}}{C_p M} \quad (2)$$

where Q_{net} is the net heat flowing into mass M per unit time, C_p is the specific heat of rock matrix, and M is the mass.

In FDEM, a heat conduction calculation model as shown in Fig. 1 is constructed. The common nodes of the triangular elements and joint elements, as nodes 1–9 show in Fig. 1, are located at the intersection the joint elements. We use the temperature of these discrete nodes to characterize the temperature field of the continuum. One-third mass of all the triangular elements that connect to one node is

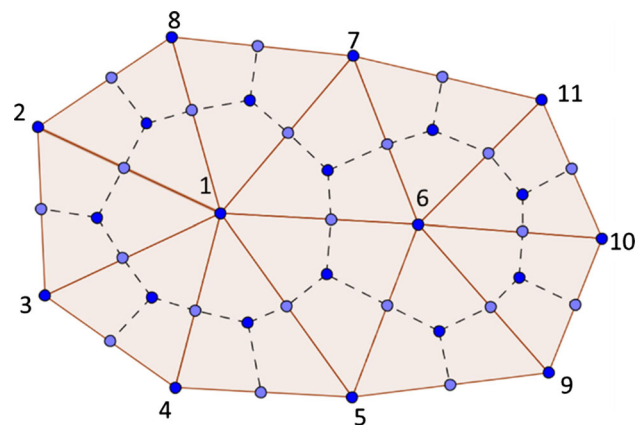


Fig. 1 Heat-transfer model of rock matrix

equivalent to the node. Here, we introduce how to calculate the temperature field of the continuum based on the topological connections shown in Fig. 1.

Taking node 1 in Fig. 1 as an example, seven triangular elements ($\Delta 123$, $\Delta 134$, $\Delta 145$, $\Delta 156$, $\Delta 167$, $\Delta 178$, and $\Delta 182$) connect to node 1. We take the polygon that surrounds node 1 as a domain, and the heat conduction calculation of the domain is equivalent to node 1. The temperature of the entire polygon region is represented by node 1. Since the temperature at nodes 2, 3, 4, 5, 6, 7 may be different from the temperature at node 1, heat conduction may occur in these regions. Here, we take one of the triangular elements $\Delta 123$ that connect to node 1 as an example. Assuming that the temperature distribution in the triangular element obeys linear distribution, the temperature gradient at any point in the triangular element is constant and can be expressed as

$$\frac{\partial T}{\partial x_i} = \frac{1}{A} \int_A \frac{\partial T}{\partial x_i} dA \tag{3}$$

According to the divergence theorem, Eq. [38] can be written as

$$\frac{\partial T}{\partial x_i} = \frac{1}{A} \int_s T n_i ds = \frac{1}{A} \sum_{m=1}^3 \bar{T}^m \in_{ij} \Delta x_j^m \tag{4}$$

where A is the area of the triangular element, n is the outer normal vector, \bar{T}^m is the average temperature of the edge m , Δx_j^m is the difference between the coordinate components of the two vertices at the edge m , and \in_{ij} is the two-dimensional permutation tensor, $\in = \begin{pmatrix} 0 & 1 \\ -1 & 0 \end{pmatrix}$.

Then, substituting Eq. [4] into Eq. [1], the heat flow rate in the x and y directions (q_x and q_y) can be obtained.

Thus, the heat flow into node 1 per unit time can be calculated by the following equation

$$Q = -\frac{q_i n_i^{(n)} L^{(n)}}{2} \tag{5}$$

where $n_i^{(n)}$ is the outer normal unit vector of the edge opposite to node n and $L^{(n)}$ is the length of the edge opposite to node n .

Thus, the heat flow $Q_{\Delta 123}$ into node 1 from the triangular element $\Delta 123$ is obtained. Similarly, the heat flow into node 1 from the other triangular elements that directly connect to the node can also be obtained. Then, the total heat flow into node 1 per unit time can be expressed as

$$Q_s = Q_{D123} + Q_{D134} + Q_{D145} + Q_{D156} + Q_{D167} + Q_{D178} + Q_{D182} \tag{6}$$

Thus, according to Eq. [2], the temperature of node 1 at the next time step is given by

$$T_{t+\Delta t}^s = T_t^s + \frac{Q_s}{C_s \rho_s V_s} \Delta t \tag{7}$$

where C_s is specific heat of rock matrix, ρ_s is the mass density of rock matrix, V_s is the rock matrix volume of the node 1.

Similarly, the temperature of other discrete nodes can be updated by the above method. Then, the evolution of the temperature field in the entire solution domain can be obtained.

Since an explicit algorithm is used in the thermal conduction calculation of this paper, the time step should be less than the critical time to ensure the numerical stability. The critical time step is given by

$$\Delta t_c = \frac{(\Delta x)^2}{4\kappa[1 + h\Delta x/2k]} \tag{8}$$

where Δx is the size of the smallest element, h is the convective heat-transfer coefficient, and κ is the thermal diffusion coefficient ($k/\rho C_p$ when $k_x = k_y$).

2.2 Fluid heat-transfer model in a fracture

As fluid flows in a fracture, the heat in fluid is transported by convection and conduction. Figure 2 shows a portion of the hydraulic fracture network formed by the broken joint elements in FDEM, where the cyan line represents the path of the fluid flow, while the triangular elements and the other joint elements do not allow fluid flow.

Taking node 1 as an example, the temperature difference between node 1 and node 2 is given by:

$$\Delta T = T_1 - T_2 \tag{9}$$

where T_1 is the temperature of node 1 and T_2 is the temperature of node 2. Then, according to Fourier’s law, the

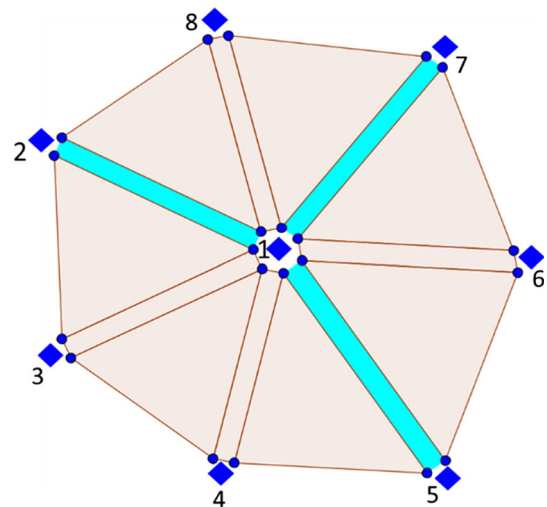


Fig. 2 Fluid heat-transfer model in fractures

heat flow rate between node 1 and node 2 caused by the heat conduction is given by

$$q_{12} = -k_f \frac{\Delta T}{L} \tag{10}$$

where k_f is the thermal conductivity of the fluid and L is the distance between the two nodes. If the temperature of node 1 is higher than that of node 2, then the heat flows out from node 1 into node 2.

Similarly, the heat flow rate between node 1 and nodes 5 or 7 can also be obtained. Finally, the total heat flow rate into node 1 due to the heat conduction is given by $Q_{f1} = q_{12} + q_{15} + q_{17}$.

2.3 Heat convection model of fluid in a fracture

In addition to heat conduction, the heat flow between two nodes can also be caused by heat convection, as shown in Fig. 2. The temperature difference between node 1 and node 2 is given by $\Delta T = T_1 - T_2$ according to Eq. [9].

The heat flow due to convection between node 1 and node 2 is given by

$$q_{12} = -0.5\rho_f C_f q_f \frac{\Delta T}{L} \tag{13}$$

where q_f is the fluid flow rate between node 1 and node 2 and can be obtained by the following approach. Assuming that the pressures at nodes 1 and 2 are p_1 and p_2 , respectively, the pressure difference between node 1 and node 2 without considering gravity is $\Delta p = p_1 - p_2$. According to the cubic law [37], the fluid flow rate between node 1 and node 2 is given by

$$q_f = -\frac{1}{12\mu} a^3 \frac{\Delta p}{L} \tag{14}$$

where μ is the dynamic viscous coefficient of the fluid and a is the aperture of the fracture.

Similarly, the heat flow rates between node 1 and nodes 5 or 7 induced by convection can also be obtained. Thus, the total heat flow rate of node 1 due to the convection of the fluid is $Q_{f2} = q_{21} + q_{41} + q_{51}$.

The temperature of node 1 at the next time step can then be updated as follows:

$$T_{t+\Delta t}^f = T_t^f + \frac{Q_f \Delta t}{C_f \rho_f V} \tag{15}$$

where T_{t+} is the temperature of node 1 at the previous time step, C_f is the specific heat of the fluid, ρ_f is the mass density of fluid, $Q_f = Q_{f1} + Q_{f2}$ is the total heat flow rate of node 1, Δt is the time step, and V_{is} is the half volume of all the broken joint elements that connect to node 1, as shown in Fig. 2.

The stability of the numerical scheme for solving the heat convection problems is governed by two numbers: the Peclet number $Pe = \rho_f q_f C_f L / k_f$ and the Courant number $C_{rg} = |v_f| \Delta t / L$, where v_f is the fluid velocity.

In the one-dimensional case, the classical constraints are $Pe \leq 2$ and $C_{rg} \leq 1$ [30]. Since the explicit fluid and thermal time steps are identical to those adopted in the conduction calculation in Sect. 2.1, the model thus sets no intrinsic limit on the Peclet number. However, the accuracy is to be different for different number values, and to be influenced by grid size and time step [9].

2.4 Heat exchange between a fluid and rock

The heat exchange between fluid and rock matrix occurs since the temperature of rock matrix and the fluid in a fracture are usually different. Here, we use the following approach to obtain the heat exchange between fluid and rock matrix, assuming that the temperature of the rock matrix at both sides of the fracture is T_s^+ and T_s^- , respectively, as shown in Fig. 3. In addition, the temperature of the fluid in the fracture is T_f , the fracture length is L , and the convective heat-transfer coefficient between the fluid and rock matrix is h . Then, the heat exchange between the fluid and rock matrix per unit time is given by

$$Q_e = h(T_s^+ - T_f)L + h(T_s^- - T_e)L \tag{16}$$

The heat-transfer calculation of the fluid in the fracture is finally updated as follows

$$T_{t+\Delta t}^f = T_t^f + \frac{(Q_f + Q_e)\Delta t}{C_p \rho_f V} \tag{17}$$

The heat-transfer calculation of the rock matrix is finally calculated using the following formula

$$T_{t+\Delta t}^s = T_t^s + \frac{(Q_s - Q_e)\Delta t}{C_p M} \tag{18}$$

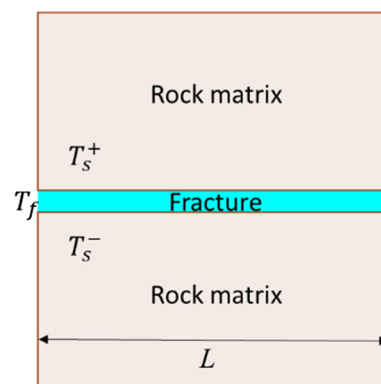


Fig. 3 Heat exchange model between fluid and rock matrix

3 Model validation

3.1 Fluid heat conduction

As shown in Fig. 4, the rock mass contains a single fracture with length of 4 m. The fracture is filled with fluid, and the fluid pressure in the fracture is uniform. The temperature at the left boundary is fixed at 100 °C, but at the right boundary the temperature is fixed at 0 °C. The other boundaries are adiabatic regardless of the thermal conductivity of rock matrix. Only heat conduction is considered for fluid in fracture. The temperature distribution of fluid in the fracture is determined by the coupled hydro-thermal model presented in this paper. The physical parameters are as follows: the mass density of fluid $\rho_f = 1000 \text{ kg/m}^3$, the thermal conductivity of fluid $k_f = 1.6 \text{ W/m } ^\circ\text{C}$, and the specific heat of fluid $C_f = 0.2 \text{ J/kg } ^\circ\text{C}$.

The analytical solution of the problem is given by [4]

$$T(x, t) = T_L + \frac{x}{L}(T_R - T_L) + \frac{2}{\pi} \sum_{n=1}^{\infty} e^{-kn^2\pi t/L^2} \left(\frac{T_R \cos(n\pi) - T_L}{n} \right) \sin \frac{n\pi x}{L} \tag{19}$$

where T_L is the temperature at the left boundary, T_R is the temperature at the right boundary, t is the time, and x is the distance to the left boundary. Furthermore, $\kappa = k_f/(\rho_f C_f)$, where k_f is the thermal conductivity of fluid, ρ_f is the mass density of fluid, and C_f is the specific heat of fluid.

Figure 5 shows the temperature distribution of fluid in the fracture at different times. It can be seen that the numerical solution agrees very well with analytical solution, verifying the correctness of the coupled hydro-thermal model in dealing with the problem of heat conduction in fluid. The temperature of fluid in the fracture gradually increases and eventually displays a linear distribution.

3.2 Heat conduction and convection of fluid in fracture

For the example in Sect. 3.1, the following two conditions are considered: [2] the fluid pressure at the left boundary is fixed at $2 \times 10^4 \text{ Pa}$, but the pressure at the right boundary is fixed at 0 Pa, and [34] the pressure at the left boundary is fixed at 0 Pa, while the fluid pressure at the right boundary

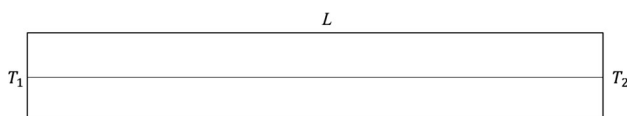


Fig. 4 Heat conduction of fluid in a single fracture

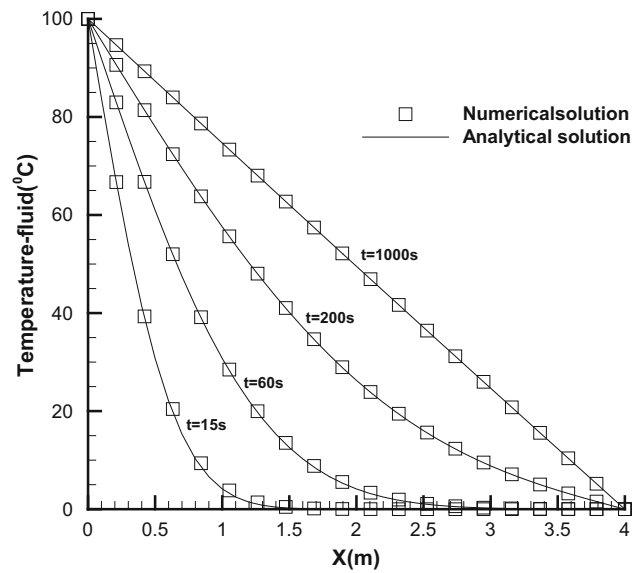


Fig. 5 Comparison of numerical solution and analytical solution

is fixed at $2 \times 10^4 \text{ Pa}$. Fluid flow occurs in the fracture and heat is transported by convection and conduction because of the pressure difference between the left and right boundaries. The coupled hydro-thermal model in this paper is used to determine the final temperature distribution of fluid in the fracture.

The analytical solution of the problem is given by [9]

$$\hat{T} = \hat{T}_R \frac{e^{P_e \hat{x}} - 1}{e^{P_e} - 1} \tag{20}$$

where $\hat{T} = (T - T_L)/T_L$, $\hat{x} = x/L$, and P_e is the Peclet number. The Peclet number is defined as

$$P_e = \rho_f C_f v_f L / k_f \tag{21}$$

where ρ_f is the mass density of fluid, C_f is the specific heat of fluid, v_f is the flow velocity of fluid, and k_f is the thermal conductivity of fluid.

The final temperature distribution obtained by the coupled hydro-thermal model is shown in Fig. 6, where the numerical solution and the analytical solution are in good agreement. In case [2], the direction of the fluid flow is the same as that of the heat conduction, accelerating heat transfer. In case [34], the flow direction of the fluid is opposite to that of the heat conduction, inhibiting heat transfer (Fig. 7).

3.3 Heat exchange between fluid and rock matrix

As shown in Fig. 8, a high-temperature rock mass is 100 m length and 100 m wide. The permeability of rock matrix is very low and has been ignored. A horizontal fracture is positioned at $x = 0$ and divides the rock mass into two

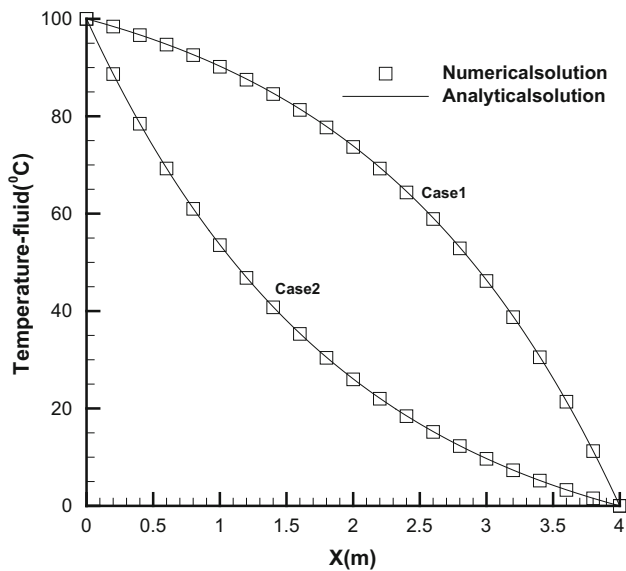


Fig. 6 Comparison of the numerical solution and analytical solution when considering heat convection of fluid

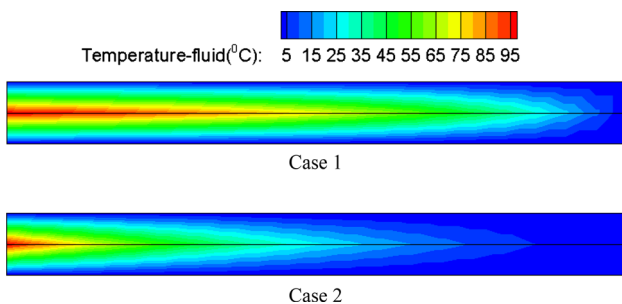


Fig. 7 Temperature distribution of fluid in the fracture

pieces. The aperture of the fracture a is 1×10^{-3} m. At the left boundary of the fracture, cold fluid is injected at a flow rate of $v_f = 0.01$ m/s. The low-temperature fluid in the fracture exchanges heat with the high-temperature rock matrix at the fracture boundary. Then, the temperature of the rock matrix around the fracture decreases. We use this example to verify the correctness of the coupled hydro-thermal model in the treatment of heat transfer between fluid and rock matrix. Since the analytical solution of the problem [6] is obtained by assuming that the problem domain is semi-infinite, the size of the numerical model should be large enough.

The temperature field evolution in rock matrix is given by

$$T_s(x, y, t) = T_{s0} + (T_{f0} - T_{s0}) \operatorname{erfc} \left[\frac{2k_s x + |y| \rho_f C_f v_f a}{2\rho_f C_f v_f a} \sqrt{\frac{\rho_s C_s v_f}{k_s(v_f t + x)}} \right] \quad (22)$$

The temperature field evolution of fluid in a fracture is given by

$$T_s(x, t) = T_{s0} + (T_{f0} - T_{s0}) \operatorname{erfc} \left[\frac{k_s x}{\rho_f C_f v_f a} \sqrt{\frac{\rho_s C_s v_f}{k_s(v_f t + x)}} \right] \quad (23)$$

where T_{s0} is the initial temperature of rock matrix, T_{f0} is the temperature of the injected fluid at the left boundary, erfc is the complementary error function, k_s is the thermal conductivity of rock matrix, ρ_f is the mass density of fluid, C_f is the specific heat of fluid, v_f is the flow velocity of fluid, ρ_s is the mass density of rock matrix, C_s is the specific heat of the rock matrix, a is the aperture of the fracture, and t is the time.

The calculation parameters used in the coupled hydro-thermal model include: the fluid mass density $\rho_f = 1000$ kg/m³, the dynamic viscosity of fluid $\mu = 1$ mPa·s, the specific heat of fluid $C_f = 4200$ J/(kg °C), the thermal conductivity of fluid $k_f = 0$ W/(m °C), the mass density of rock matrix $\rho_s = 2700$ kg/m³, the specific heat of rock matrix $C_s = 1000$ J/(kg °C), the thermal conductivity of rock matrix $k_s = 3$ W/(m °C), and the aperture of the fracture $a = 1 \times 10^{-3}$ m. The convective heat-transfer coefficient between fluid and rock matrix h will be discussed in detail. To facilitate the analysis of the temperature distribution within rock matrix, we set two monitoring lines at $x = 2$ m and $y = 2$ m, as shown in Fig. 8.

In the analytical solution, the temperature of fluid in the fracture is assumed to be equal to the temperature of the rock matrix at the boundary of the fracture. This boundary condition can be regarded as a special case of convective boundary condition in the coupled hydro-thermal model. The correct numerical results should converge to the analytical solution as the convective heat-transfer coefficient increases. Thus, we first discuss the value of the convective heat-transfer coefficient h . For three different convective heat-transfer coefficients $h = 10, 100,$ and 1000 W/(m² °C), the temperature distribution of fluid in the fracture at $t = 10$ d is obtained by the coupled hydro-thermal model. As shown in Fig. 9, the numerical solution is still quite different from the analytical solution when $h = 10$ W/(m² °C). However, the difference between the numerical solution and analytical solution is very small when $h = 100$ W/(m² °C). For $h = 1000$ W/(m² °C), the numerical solution is completely consistent with the analytical solution. Therefore, we take $h = 1000$ W/(m² °C) in the subsequent validation calculations in order to compare the numerical solution with the analytical solution.

For $h = 1000$ W/(m² °C), the temperature evolution at different locations obtained by the coupled hydro-thermal model is shown in Fig. 10. It can be seen that the

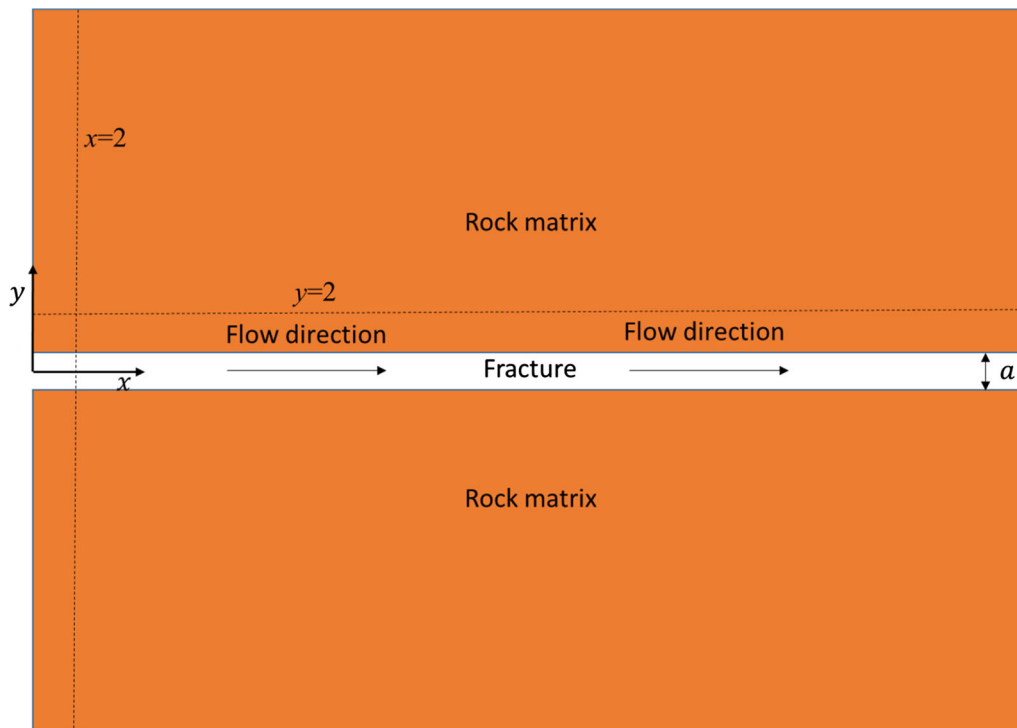


Fig. 8 A single fracture model for simulating the heat transfer between fluid and rock matrix

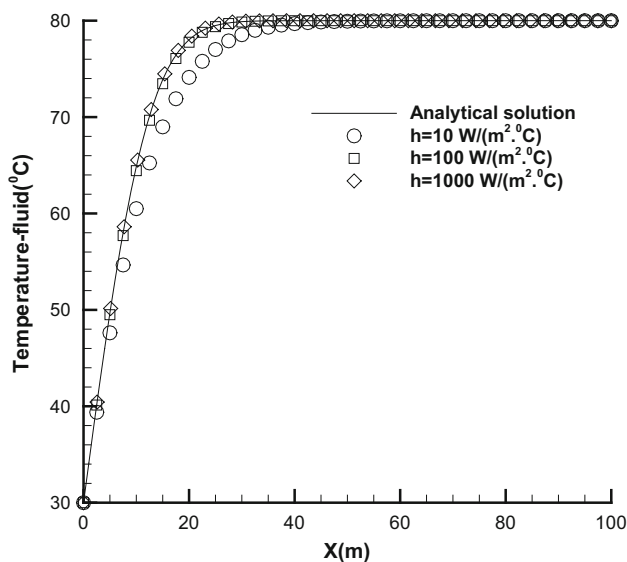


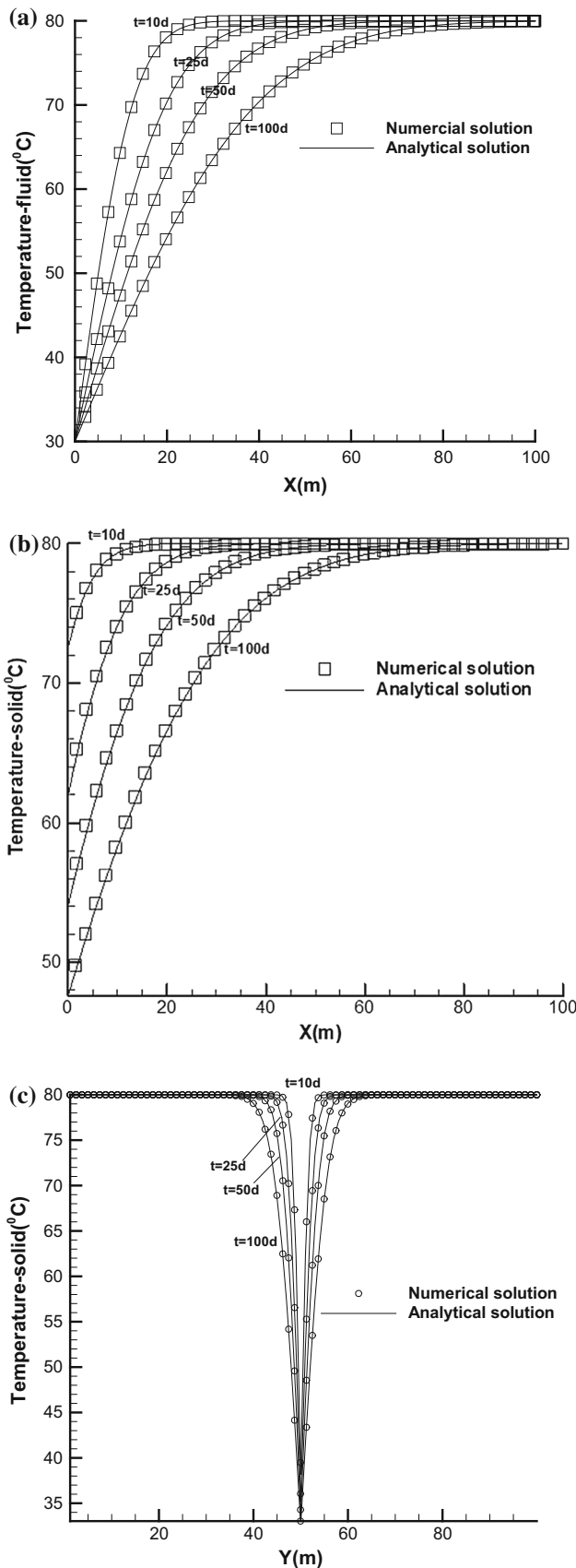
Fig. 9 Comparison of the numerical solution and analytical solution at $t = 10$ d when the convective heat-transfer coefficient between fluid and rock matrix h is 10, 100, and 1000 $\text{W}/(\text{m}^2 \cdot ^\circ\text{C})$

temperature distribution of fluid in the fracture and the temperature distribution along the monitoring line in the rock matrix are both consistent with the analytical solution, verifying the correctness of the coupled hydro-thermal model in simulating the heat exchange between fluid and rock matrix.

4 Hydro-thermal coupling in the rock mass with a fracture network

4.1 Model and parameters

The coupled hydro-thermal model presented in this paper is used to predict the heat transport and fluid flow in the rock mass with a fracture network from the literature [31]. As shown in Fig. 11, seven through-going fractures (J2, J5, J6, J7, J8, J9, and J10) and five non-through-going fractures (J1, J3, J4, J11, and J12) exist in the square region with the edge length of 10 m. In this calculation, only the hydro-thermal coupling is considered. The boundary conditions are as follows (1). Seepage field: fluid pressure at the left boundary (inlet) is fixed at 200 kPa, while the fluid pressure at the right boundary (outlet) is fixed at 100 kPa; the top and bottom boundaries are impermeable. (2) Temperature field: the temperature of the injected fluid at the left boundary is fixed at 20 $^\circ\text{C}$, and the top and bottom boundaries are both adiabatic. The initial temperature of rock matrix and fluid is both 80 $^\circ\text{C}$. The time step of the hydro-thermal coupling calculation is 0.5 s. The square region is discretized into 2380 triangular elements. The calculated parameters include: $\rho_f = 1000 \text{ kg}/\text{m}^3$, the dynamic viscosity of fluid $\mu = 1 \text{ mPa}\cdot\text{s}$, the specific heat of fluid $C_f = 4200 \text{ J}/(\text{kg} \cdot ^\circ\text{C})$, the thermal conductivity of fluid $k_f = 0 \text{ W}/(\text{m} \cdot ^\circ\text{C})$, the mass density of rock matrix $\rho_s = 2700 \text{ kg}/\text{m}^3$, the specific heat of rock matrix



◀Fig. 10 Comparison of the numerical solution and analytical solution of the temperature distribution in fluid and rock matrix: **a** the temperature distribution of fluid in fractures, **b** the temperature distribution in rock matrix at the horizontal monitoring line $y = 2$ m, **c** the temperature distribution in rock matrix at the vertical monitoring line $x = 2$ m

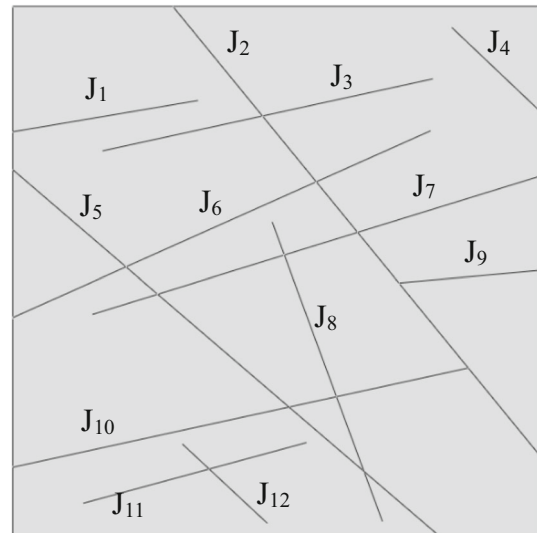


Fig. 11 Two-dimensional fracture network model

$C_S = 1000 \text{ J/(kg } ^\circ\text{C)}$, the thermal conductivity of rock matrix $k_S = 3 \text{ W/(m } ^\circ\text{C)}$, the fracture aperture $a = 5 \times 10^{-4} \text{ m}$, and the convective heat-transfer coefficient between fluid and rock matrix $h = 900 \text{ W/(m}^2 \text{ } ^\circ\text{C)}$. The heat-transfer process in rock matrix and fluid in the fracture network is simulated by the coupled hydro-thermal model presented in this paper.

4.2 Numerical simulation results

4.2.1 Seepage field

As shown in Fig. 12a, the completely isolated non-through-going fractures (J11 and J12) do not connect to the left or right boundary, and thus, the fluid pressures in them are both zero. Although the non-through-going fractures (J1, J3, and J4) that connect with the left or right boundaries or other through-going fractures, the fluid pressure within them is uniformly distributed with no pressure change along the fracture. As shown in Fig. 12b, the flow velocity of fluid in the five non-through-going fractures is both zero. Thus, the convective heat transfer does not exist in these fractures. Therefore, the non-through-going fractures do not affect the heat-transfer calculation. The simulation result of the temperature field will confirm the above-mentioned interpretations.

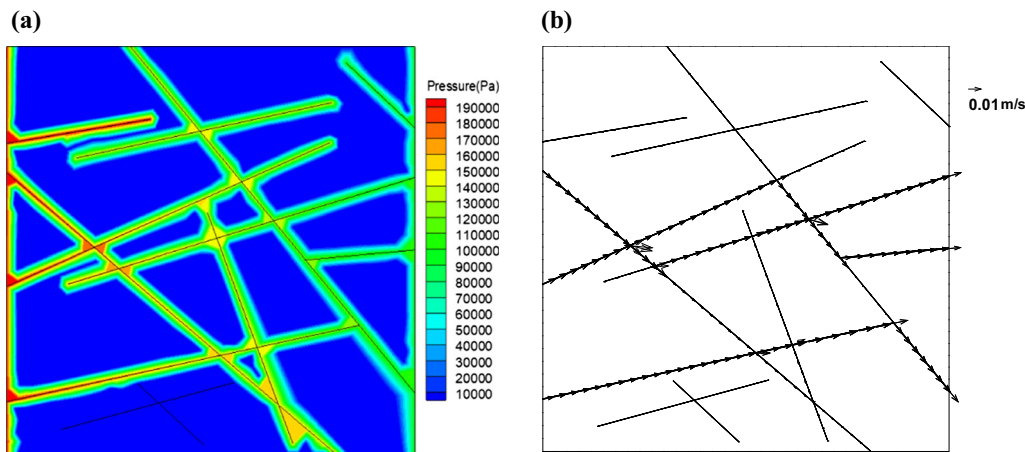


Fig. 12 Fluid pressure distribution and velocity distribution at a stable seepage: **a** fluid pressure distribution, **b** flow velocity distribution

4.2.2 Temperature field

As the cold fluid injected into fractures, heat is transferred from the high-temperature rock matrix into fluid in fractures and is also transferred by the fluid through convective heat transfer. The rock matrix temperature decreases very fast near fractures, while the temperature of the rock matrix far from fractures decreases slowly. In Fig. 13, the through-going fractures form a channel of fluid flow, and the cold fronts move very fast along those through-going fractures and reach the right boundary quickly. As shown in Fig. 13 at 2.32 d–23.15 d, the cold fronts preferentially move along the through-going fractures J5, J6, and J10 and reach the right boundary via the through-going fractures J2, J7, and J9. The non-through-going fractures J1, J3, J4, J11, and J12 do not affect the heat transfer in the region, as shown in Fig. 13 at 57.87 d. Because the flow velocity of the fluid in the non-through-going fractures is both zero when the fluid flow is stable, as shown in Fig. 12b), heat convection in fluid does not occur. The cold fronts move quickly and reach the right boundary, which constitutes an early thermal breakthrough [3] and is disadvantageous in the utilization of geothermal resources, as shown in Fig. 13 at 57.87 d. Although the fluid temperature at the right boundary is low, the temperature of the rock matrix at the upper right corner is still high, as shown in Fig. 13 at 115.74 d. The high-temperature rock matrix continues to supply heat for fluid in fractures; consequently, the fluid temperature at the outlet does not drop rapidly to the inlet temperature but gradually decreases after a long period of time (i.e., the so-called long-tail effect).

For the convenience of subsequent discussions, the average fluid temperature at the outlet is defined here [3]

$$T_{\text{out}} = \frac{\sum v_{\text{frac}} a T_{\text{frac}} + \int v T \, dy}{\sum v_{\text{frac}} a + \int v \, dy} \quad (24)$$

where v is the flow velocity and the subscript frac represents the fracture. The addition term represents the fracture, while the integral term represents rock matrix. Since the permeability of rock matrix is not considered in this paper, the fluid velocity in rock matrix is zero. Thus, Eq. [16] can be written as

$$T_{\text{out}} = \frac{\sum v_{\text{frac}} a T_{\text{frac}}}{\sum v_{\text{frac}} a} \quad (25)$$

4.2.3 Influence of the thermal conductivity of rock matrix on the outlet fluid temperature

The thermal conductivities $k = 0.5, 1.0, 2.0,$ and $3.0 \text{ W/(m } ^\circ\text{C)}$ were used to study the effect of the thermal conductivity of rock matrix on the thermal breakthrough curve. As shown in Fig. 14, the greater the thermal conductivity of rock matrix is, the later the thermal breakthrough occurs, and the less obvious the long-tail effect. The outlet fluid temperature decreases with decreasing rock matrix. After a period of time, the outlet fluid temperature is higher than that of rock matrix with high thermal conductivity. The thermal conductivity of rock matrix determines the time when the temperature of fluid and rock matrix is balanced. If the thermal conductivity of the rock matrix is low, then the initially high-temperature rock matrix heats the low-temperature fluid in fractures slowly. Thus, the heat breakthrough occurs early. After a period of time, the energy stored in the rock matrix is less absorbed by fluid in fractures. Thus, the outlet temperature at the late stage is higher than that when the thermal conductivity of rock matrix is high.

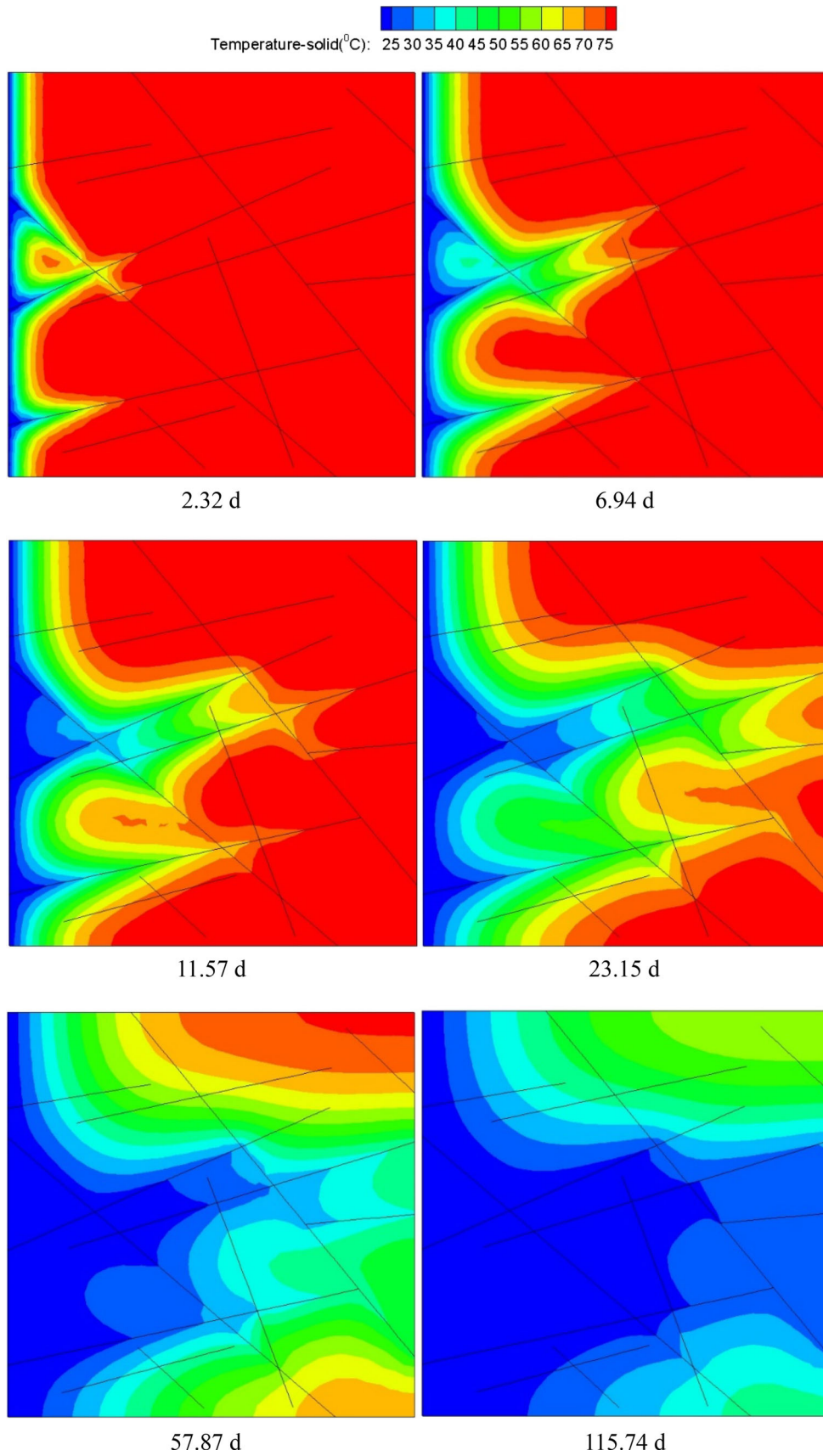


Fig. 13 Temperature distribution at different times

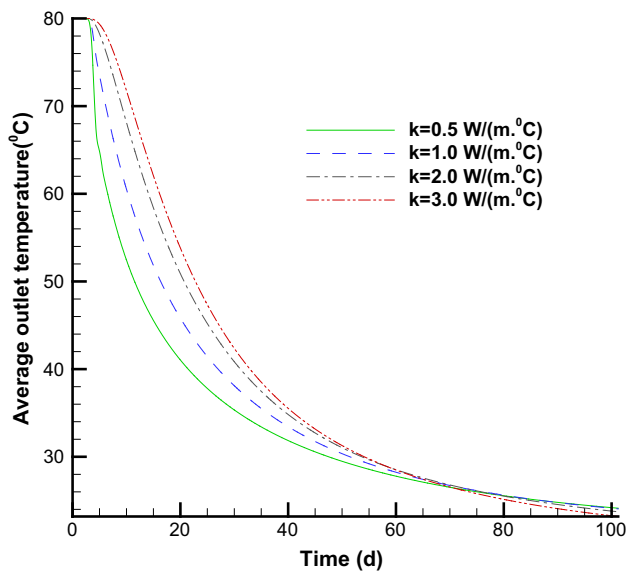


Fig. 14 Effect of the thermal conductivity of rock matrix on the outlet fluid temperature

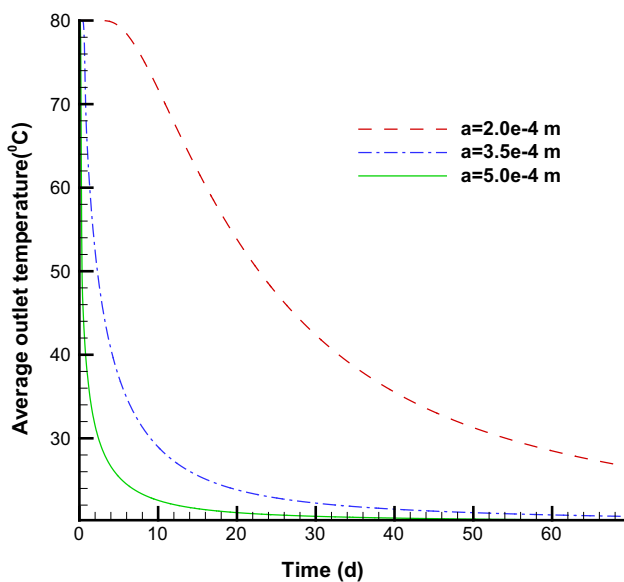


Fig. 15 Effect of fracture aperture on the outlet fluid temperature

4.2.4 The effect of fracture aperture on the outlet fluid temperature

Fractures are mainly caused by hydraulic fracturing during construction of the reservoir. Fracture aperture is closely related to fluid circulation impedance, fluid short circuit, heat production efficiency and reservoir life. If the flow rate is constant, the fracture aperture determines the amount of fluid in the fracture and the ability to extract heat from rock matrix. The fracture aperture also determines the heating time and the fracture path length that heats fluid to

a specific temperature. Figure 15 shows the variation of the outlet fluid temperature with time when $a = 2 \times 10^{-4}$, 3.5×10^{-4} , and 5×10^{-4} m. As can be seen from this figure, the wider the fracture aperture is, the earlier the thermal breakthrough occurs, and the less obvious the long-tail effect. Moreover, the fluid temperature decreases faster as the fracture aperture increases. Because the flow rate of the fluid in fracture with large aperture is larger than that with small aperture under the same boundary conditions, the fluid is not heated sufficiently when it flows out of the right boundary. Finally, the fluid temperature at the outlet decreases rapidly.

5 Conclusion

In this paper, a two-dimensional coupled hydro-thermal (FDEM-TH) model for FDEM is constructed. Three examples with analytical solutions are given to verify the correctness of the coupled model. The numerical results agree well with the analytical results. Finally, a hydro-thermal coupling example of rock mass with a fracture network is given. The results show that heat is transferred from high-temperature rock matrix to cold fluid in fractures and is carried away by the heat convection of fluid. The temperature of rock matrix near fractures decreases rapidly, while the temperature of rock matrix far from fractures decreases slowly. The thermal breakthrough occurs late if the thermal conductivity of rock matrix is high, and the long-tail effect is obvious. But if the fracture aperture is large, the long-tail effect is not obvious. This coupled hydro-thermal model combined with the mechanical fracture calculation of FDEM can construct a complete method for simulating rock rupture driven by the effect of THM coupling.

Acknowledgements This work was supported by the National Natural Science Foundation of China under the Grant Number 11602006; the Beijing Natural Science Foundation under the Grant Number 1174012; the Fundamental Research Funds for the Central Universities, China University of Geosciences (Wuhan); the Chaoyang District Postdoctoral Science Foundation funded project under the Grant Number 2016ZZ-01-08; and the National Natural Science Foundation of China under Grant Number 41731284, 11672360 and 51479191.

References

1. Abdallah G, Thoraval A, Sfeir A, Piguet J-P (1995) Thermal convection of fluid in fractured media. In: International journal of rock mechanics and mining sciences & geomechanics abstracts, vol 5. Elsevier, pp 481–490
2. Barton N, Bandis S, Bakhtar K (1985) Strength, deformation and conductivity coupling of rock joints. In: International journal of rock mechanics and mining sciences & geomechanics Abstracts, vol 3. Elsevier, pp 121–140

3. Chen B, Song E, Cheng X (2014) A numerical method for discrete fracture network model for flow and heat transfer in two-dimensional fractured rocks. *Chin J Rock Mech Eng* 33(1):43–51
4. Crank J (1975) *The mathematics of diffusion*, 2nd edn. Oxford University Press, Oxford
5. Cui W, Gawecka KA, Potts DM, Taborda DMG, Zdravković L (2016) Numerical analysis of coupled thermo-hydraulic problems in geotechnical engineering. *Geomech Energy Environ* 6:22–34. <https://doi.org/10.1016/j.gete.2016.03.002>
6. Hu J, Su Z, Wu N-Y, H-z Zhai, Y-c Zeng (2014) Analysis on temperature fields of thermal-hydraulic coupled fluid and rock in enhanced geothermal system. *Progress Geophys* 29(3):1391–1398
7. Hudson J, Stephansson O, Andersson J, Tsang C-F, Jing L (2001) Coupled T–H–M issues relating to radioactive waste repository design and performance. *Int J Rock Mech Min Sci* 38(1):143–161
8. Inc ICG (2005) Code PFC. User's Guide, Minnesota, USA. 2005
9. Itasca (2005) Consulting Group Inc, Code 3DEC. User's Guide, Minnesota, USA
10. Itasca Consulting Group Inc (2005) Code UDEC. User's Guide, Minnesota, USA
11. Itasca Consulting Group Inc (2005) Code FLAC. User's Guide, Minnesota, USA
12. Jiang F, Chen J, Huang W, Luo L (2014) A three-dimensional transient model for EGS subsurface thermo-hydraulic process. *Energy* 72:300–310. <https://doi.org/10.1016/j.energy.2014.05.038>
13. Jing L, Tsang C-F, Stephansson O (1995) DECOVALEX—an international co-operative research project on mathematical models of coupled THM processes for safety analysis of radioactive waste repositories. In: *International journal of rock mechanics and mining sciences & geomechanics abstracts*, vol 5. Elsevier, pp 389–398
14. Latham J-P, Xiang J, Belayneh M, Nick HM, Tsang C-F, Blunt MJ (2013) Modelling stress-dependent permeability in fractured rock including effects of propagating and bending fractures. *Int J Rock Mech Min Sci* 57:100–112. <https://doi.org/10.1016/j.ijrmmms.2012.08.002>
15. Lei Z, Rougier E, Knight EE, Munjiza A (2014) A framework for grand scale parallelization of the combined finite discrete element method in 2d. *Comput Part Mech* 1(3):307–319. <https://doi.org/10.1007/s40571-014-0026-3>
16. Lei Z, Rougier E, Knight EE, Munjiza A (2015) FDEM Simulation on Fracture Coalescence in Brittle Materials. In: Paper presented at the 49th US Rock Mechanics/Geomechanics Symposium
17. Lei Q, Latham J-P, Xiang J, Tsang C-F (2015) Polyaxial stress-induced variable aperture model for persistent 3D fracture networks. *Geomech Energy Environ* 1:34–47. <https://doi.org/10.1016/j.gete.2015.03.003>
18. Lei Q, Latham J-P, Xiang J (2016) Implementation of an empirical joint constitutive model into finite-discrete element analysis of the geomechanical behaviour of fractured rocks. *Rock Mech Rock Eng* 49(12):4799–4816. <https://doi.org/10.1007/s00603-016-1064-3>
19. Lei Z, Rougier E, Knight EE, Frash L, Carey JW, Viswanathan H (2016) A non-locking composite tetrahedron element for the combined finite discrete element method. *Eng Comput* 33(7):1929–1956. <https://doi.org/10.1108/ec-09-2015-0268>
20. Lei Z, Rougier E, Knight EE, Munjiza A, Viswanathan H (2016) A generalized anisotropic deformation formulation for geomaterials. *Comput Part Mech* 3(2):215–228. <https://doi.org/10.1007/s40571-015-0079-y>
21. Lisjak A, Grasselli G, Vietor T (2014) Continuum–discontinuum analysis of failure mechanisms around unsupported circular excavations in anisotropic clay shales. *Int J Rock Mech Min Sci* 65:96–115. <https://doi.org/10.1016/j.ijrmmms.2013.10.006>
22. Lisjak A, Tatone BSA, Grasselli G, Vietor T (2014) Numerical modelling of the anisotropic mechanical behaviour of opalinus clay at the laboratory-scale using fem/DEM. *Rock Mech Rock Eng* 47(1):187–206. <https://doi.org/10.1007/s00603-012-0354-7>
23. Lisjak A, Tatone BSA, Mahabadi OK, Grasselli G, Marschall P, Lanyon GW, Rdl Vaissière, Shao H, Leung H, Nussbaum C (2016) Hybrid finite-discrete element simulation of the EDZ formation and mechanical sealing process around a microtunnel in Opalinus Clay. *Rock Mech Rock Eng* 49(5):1849–1873. <https://doi.org/10.1007/s00603-015-0847-2>
24. Lisjak A, Kaifosh P, He L, Tatone BSA, Mahabadi OK, Grasselli G (2017) A 2D, fully-coupled, hydro-mechanical, FDEM formulation for modelling fracturing processes in discontinuous, porous rock masses. *Comput Geotech* 81:1–18. <https://doi.org/10.1016/j.compgeo.2016.07.009>
25. Mahabadi O, Kaifosh P, Marschall P, Vietor T (2014) Three-dimensional FDEM numerical simulation of failure processes observed in Opalinus Clay laboratory samples. *J Rock Mech Geotech Eng* 6(6):591–606. <https://doi.org/10.1016/j.jrmge.2014.10.005>
26. Munjiza A (2004) *The combined finite-discrete element method*. Wiley, London
27. Munjiza A (2011) *Computational mechanics of discontinua*. Wiley, Hoboken
28. Munjiza A, Owen DRJ, Bicanic N (1995) A combined finite-discrete element method in transient dynamics of fracturing solids. *Eng Comput* 12(2):145–174. <https://doi.org/10.1108/02644409510799532>
29. Munjiza A, Latham J, Andrews K (2000) Detonation gas model for combined finite-discrete element simulation of fracture and fragmentation. *Int J Numer Methods Eng* 49(12):1495–1520
30. Perrochet P, Béro D (1993) Stability of the standard Crank-Nicolson-Galerkin Scheme applied to the diffusion-convection equation: some new insights. *Water Resour Res* 29(9):3291–3297
31. Priest SD (2012) *Discontinuity analysis for rock engineering*. Springer, Berlin
32. Pruess K (1983) Heat transfer in fractured geothermal reservoirs with boiling. *Water Resour Res* 19(1):201–208
33. Rougier E, Knight EE, Broome ST, Sussman AJ, Munjiza A (2014) Validation of a three-dimensional finite-discrete element method using experimental results of the split Hopkinson pressure bar test. *Int J Rock Mech Min Sci* 70:101–108. <https://doi.org/10.1016/j.ijrmmms.2014.03.011>
34. Rutqvist J (2011) Status of the TOUGH-FLAC simulator and recent applications related to coupled fluid flow and crustal deformations. *Comput Geosci* 37(6):739–750. <https://doi.org/10.1016/j.cageo.2010.08.006>
35. Senseney CT, Duan Z, Zhang B, Regueiro RA (2017) Combined spheropolyhedral discrete element (DE)–finite element (FE) computational modeling of vertical plate loading on cohesionless soil. *Acta Geotech* 12(3):593–603. <https://doi.org/10.1007/s11440-016-0519-8>
36. Shaik AR, Rahman SS, Tran NH, Tran T (2011) Numerical simulation of fluid-rock coupling heat transfer in naturally fractured geothermal system. *Appl Therm Eng* 31(10):1600–1606. <https://doi.org/10.1016/j.applthermaleng.2011.01.038>
37. Snow DT (1965) A parallel plate model of fractured permeable media. Ph.D. Thesis, Univ of California
38. Sun Z-x, Zhang X, Xu Y, Yao J, Wang H-x, Lv S, Sun Z-l, Huang Y, Cai M-y, Huang X (2017) Numerical simulation of the heat extraction in EGS with thermal-hydraulic-mechanical coupling method based on discrete fractures model. *Energy* 120:20–33. <https://doi.org/10.1016/j.energy.2016.10.046>
39. Tomac I, Gutierrez M (2015) Formulation and implementation of coupled forced heat convection and heat conduction in DEM.

- Acta Geotech 10(4):421–433. <https://doi.org/10.1007/s11440-015-0400-1>
40. Tsang C-F, Stephansson O, Jing L, Kautsky F (2009) DECOVALEX Project: from 1992 to 2007. *Environ Geol* 57(6):1221–1237
 41. Xu T, Zhang Y, Yu Z, Hu Z, Guo L (2015) Laboratory study of hydraulic fracturing on hot dry rock. *Sci Technol Rev* 33(19):35–39
 42. Xu C, Dowd PA, Tian ZF (2015) A simplified coupled hydro-thermal model for enhanced geothermal systems. *Appl Energy* 140:135–145. <https://doi.org/10.1016/j.apenergy.2014.11.050>
 43. Yan C, Zheng H (2016) A two-dimensional coupled hydro-mechanical finite-discrete model considering porous media flow for simulating hydraulic fracturing. *Int J Rock Mech Min Sci* 88:115–128. <https://doi.org/10.1016/j.ijrmms.2016.07.019>
 44. Yan C, Zheng H (2017) A coupled thermo-mechanical model based on the combined finite-discrete element method for simulating thermal cracking of rock. *Int J Rock Mech Min Sci* 91:170–178. <https://doi.org/10.1016/j.ijrmms.2016.11.023>
 45. Yan C, Zheng H (2017) Three-dimensional hydromechanical model of hydraulic fracturing with arbitrarily discrete fracture networks using finite-discrete element method. *Int J Geomech* 17(6):04016133
 46. Yan C, Zheng H (2017) FDEM-flow3D: a 3D hydro-mechanical coupled model considering the pore seepage of rock matrix for simulating three-dimensional hydraulic fracturing. *Comput Geotech* 81:212–228. <https://doi.org/10.1016/j.compgeo.2016.08.014>
 47. Yan C, Zheng H, Sun G, Ge X (2016) Combined finite-discrete element method for simulation of hydraulic fracturing. *Rock Mech Rock Eng* 49(4):1389–1410. <https://doi.org/10.1007/s00603-015-0816-9>
 48. Zhao J (1993) Convective heat transfer and water flow in rough granite fractures. In: *ISRM international symposium-EUROCK 93*, international society for rock mechanics

Publisher's Note

Springer Nature remains neutral with regard to jurisdictional claims in published maps and institutional affiliations.